

Original Article

Metformin reduces pleural fibroelastosis by inhibition of extracellular matrix production induced by CD90-positive myofibroblasts

Yoichiro Aoshima^{1,2}, Yasunori Enomoto^{1,3}, Atsuki Fukada^{1,2}, Yuki Kurita¹, Sayomi Matsushima^{1,2}, Shiori Meguro¹, Isao Kosugi¹, Hideya Kawasaki^{1,4}, Hiroaki Katsura³, Tomoyuki Fujisawa², Noriyuki Enomoto², Yutaro Nakamura², Naoki Inui^{2,5}, Takafumi Suda², Toshihide Iwashita¹

¹Department of Regenerative and Infectious Pathology, Hamamatsu University School of Medicine, Shizuoka 431-3192, Japan; ²Second Division, Department of Internal Medicine, Hamamatsu University School of Medicine, Shizuoka 431-3192, Japan; ³Laboratory for Lung Development and Regeneration, Riken Center for Biosystems Dynamics Research (BDR), Kobe 650-0047, Japan; ⁴Preeminent Medical Photonics Education and Research Center Institute for NanoSuit Research, Hamamatsu University School of Medicine, Shizuoka 431-3192, Japan; ⁵Department of Clinical Pharmacology and Therapeutics, Hamamatsu University School of Medicine, Shizuoka 431-3192, Japan

Received July 29, 2021; Accepted October 1, 2021; Epub November 15, 2021; Published November 30, 2021

Abstract: Metformin, an AMP-activated protein kinase activator used to treat diabetes mellitus, has recently attracted attention as a promising anti-fibrotic agent. However, its anti-fibrotic effects on pleural fibroelastosis remain unknown. We induced mouse pleural fibroelastosis by intra-pleural coadministration of bleomycin and carbon and evaluated its validity as a preclinical model for human pleural fibrosis. We assessed the expression of the myofibroblast surface marker CD90 in the fibrotic pleura and the effects of metformin *in vivo* and *in vitro*. Finally, we evaluated the effects of metformin on human pleural mesothelial cells stimulated by transforming growth factor β 1 (TGF β 1). The fibrotic pleura in mice had collagen and elastin fiber deposition similar to that seen in human fibrotic pleura. Moreover, CD90-positive myofibroblasts were detected in and successfully isolated from the fibrotic pleura. Metformin significantly suppressed the deposition of collagen and elastic fibers in the fibrotic pleura and decreased the expression of extracellular matrix (ECM)-related genes, including *Col1a1*, *Col3a1*, *Fn1*, and *Eln*, in pleural CD90-positive myofibroblasts. In human pleural mesothelial cells, metformin decreased TGF β 1-induced upregulation of ECM-related genes and *SNAIL*. Overall, metformin suppresses pleural fibroelastosis by inhibition of ECM production by pleural myofibroblasts, suggesting that this drug has therapeutic potential against human pleural fibrosis, including pleuroparenchymal fibroelastosis.

Keywords: Metformin, myofibroblast, pleural fibrosis, pleuroparenchymal fibroelastosis

Introduction

Organ fibrosis is a condition in which fibroblasts and myofibroblasts produce excessive extracellular matrix (ECM) proteins such as collagen and elastin, occurring in various life-threatening diseases such as interstitial lung disease, viral and alcoholic chronic liver disease, and chronic nephrosclerosis [1]. Therefore, there is increasing interest in the development of therapeutic agents for this condition.

Pleural fibrosis occurs in the visceral pleura of the lungs. It is observed in several diseases,

including asbestos-related diffuse pleural fibrosis, pleural infections, such as tuberculous pleurisy, rheumatoid pleurisy, and hemothorax [2]. Pleuroparenchymal fibroelastosis (PPFE) has recently been recognized as a rare form of idiopathic interstitial pneumonia featuring fibrosis and severe elastosis of the pleura and subpleural lung parenchyma, particularly in the upper lobes. Patients with idiopathic PPFE experience a rapid decline in respiratory function and have an associated poor prognosis, with a survival of approximately 3 years after diagnosis [3-9]. Therefore, PPFE is one of the most critical pleural fibrotic diseases, but unfor-

Unfortunately, effective treatments for PPF and pleural/subpleural fibroelastosis have not yet been established.

Metformin, an AMP-activated protein kinase (AMPK) activator commonly used to treat diabetes mellitus, has recently attracted attention due to its anti-fibrotic effects. Specifically, it suppresses mouse lung fibrosis induced by intratracheal administration of bleomycin and decreases collagen production in (myo)fibroblasts isolated from patients with idiopathic pulmonary fibrosis (IPF) [10-14]. In addition, metformin has universal anti-fibrotic effects on multiple organs in rodent experimental fibrosis models, including the kidney [15], heart [16], liver [17], skin [18] and ovaries [19]. However, its effect on pleural fibrosis remains unknown.

In this study, we used a mouse model of pleural fibrosis induced by intra-pleural coadministration of bleomycin and carbon [20] and re-evaluated its similarities and differences with human lungs of pleural fibrosis. Then, we investigated the application of metformin as an anti-fibrotic or anti-fibroelastic agent against human pleural fibrotic diseases, including PPF, using this mouse model and human mesothelial cells.

Materials and methods

Animal experiments

C57BL/6 male wild-type mice (12-16 weeks old; approximately 25 g body weight) were purchased from SLC (Shizuoka, Japan). The mice were bred and housed in a pathogen-free mouse facility at constant temperature and humidity under a 12-h light/12-h dark cycle in sterilized plastic cages containing wood chip bedding, with *ad libitum* access to water and food.

Induction of pleural fibrosis in a mouse model by intra-pleural coadministration of bleomycin and carbon (pleural fibrosis model)

To induce pleural fibrosis in mice, we administered bleomycin (3 mg/kg; Wako, Osaka, Japan) and carbon particles (0.1 mg; carbon black 101, 90 nm diameter; Degussa, Frankfurt, Germany) in 50 μ L of sterile phosphate-buffered saline (PBS) with a single, right-sided, intra-pleural injection using a 26-gauge needle

[20]. To investigate the anti-fibrotic effects of metformin on pleural fibrosis, metformin (62.5 mg/kg; Sumitomo Dainippon Pharma, Tokyo, Japan) or PBS was intra-peritoneally injected every other day beginning on day 10 after the bleomycin/carbon administration until day 21. The dosage of metformin was determined based on a recent study [11].

Induction of lung parenchymal fibrosis by intratracheal administration of bleomycin (lung fibrosis model)

To induce lung parenchymal fibrosis, we anesthetized mice and administered a single intratracheal injection of 2 mg/kg bleomycin sulphate (Nippon Kayaku, Tokyo, Japan) in 50 μ L of sterile PBS using a MicroSprayer™ (Penn-Century, PA, USA) [21]. The lungs and lung (myo)fibroblasts were harvested on days 14 (for FACS) or 21 (for lung sections) after bleomycin administration.

Staining and immunohistochemistry (IHC) of lung tissue

Sequential 4 μ m-thick sections were cut from lung samples fixed in 4% or 10% formalin and embedded in paraffin for hematoxylin and eosin (H&E) staining, Elastica van Gieson (EVG) staining, Sirius Red staining, and Victoria Blue staining. IHC was performed as previously described [21-23]. Antigen retrieval was performed at pH 9, and the antibodies used are summarized in **Table 1**. The slides were imaged using a BX51 microscope. For Sirius Red staining under polarized light, the slides were imaged using a BX53 microscope with True Color LED (Olympus, Tokyo, Japan). Images were processed using the CellSens software (Olympus).

Immunofluorescence

Frozen lung sections: Lung samples obtained from mice were placed in an optimal cutting temperature formulation (Sakura Finetek, Tokyo, Japan), frozen at -80°C in an organic solvent and cut in 6 μ m slices at -20°C using a cryostat. The slices were fixed in cold acetone for 10 min and dried at 25°C for 20 min. Sections were incubated at 25°C for 30 min in blocking solution without detergent (10% goat serum in PBS) and then incubated with the appropriate primary antibodies (**Table 1**) and 1

Metformin reduces pleural fibroelastosis

Table 1. Antibody details used in this study

Primary antibody	Fluorescence	Clone	Supplier	Application	Dilution
Anti-CD31 (cell surface marker for vascular endothelial cells)	APC	390	BioLegend	FACS/IF	150
Anti-CD45 (cell surface marker for haematopoietic cells)	APC	30-F11	BioLegend	FACS/IF	150
Anti-CD146 (cell surface marker for pericytes and smooth muscle cells)	APC	ME-9F1	BioLegend	FACS/IF	150
Anti-E-cadherin (CD324) (cell surface marker for epithelial cells)	APC	DECMA-1	BioLegend	FACS/IF	100
Anti-LYVE1 (cell surface marker for lymphatic endothelial cells)	APC	223322	R&D SYSTEM	FACS/IF	60
Anti-TER-119 (cell surface marker for erythrocytes)	APC	TER-119	eBioscience	FACS/IF	150
Anti-Thy-1.2 (CD90.2)	FITC	53-2.1	BioLegend	FACS/IF	150
Anti-PDGFR α (CD140a) (cell surface marker for fibroblast/myofibroblast)	PE	APA5	BioLegend	FACS	50
Anti-CD34	PE	RAM34	Thermo Fisher	FACS	50
Anti-PDGFR β (CD140b)	PE	APB5	Thermo Fisher	FACS	50
Anti- α SMA	No	1A4	Sigma-Aldrich	IHC/IF	500
Anti-CD31	No	EPR17259	Abcam	IHC	1000
Anti-CD45	No	EPR20033	Abcam	IHC	2000
Anti-E-cadherin (CD324)	No		GeneTex	IHC	300
Anti-CD146	No	EPR3208	Abcam	IHC	200
Anti-LYVE1	No	EPR21771	Abcam	IHC	4000
Anti-PDGFR α (CD140a)	No	EPR5480	Abcam	IHC	100
Anti-CD3	No	SP7	Abcam	IF	100
Anti-fibronectin (Fn1)	No	EPR23110-46	Abcam	IHC	2000
Anti-phospho-SMAD2/3	No	D27F4	Cell Signaling	IF	2000*
Anti-CD90	No		Sigma-Aldrich	IHC/IF	200
Anti-WT1	No	EPR23963-116	Abcam	IF	500

IF: Immunofluorescence; IHC: Immunohistochemistry. *, Amplification required.

μ g/mL DAPI in blocking solution at 25°C for 30 min. Finally, the sections were washed in PBS and imaged.

Formalin-fixed, paraffin-embedded lung sections: Multiplex immunofluorescence staining of paraffin-embedded tissues was performed with the Opal™ 4-Color Manual IHC Kit (Perkin Elmer, Waltham, MA, USA), in which individual tyramide signal amplification-conjugated fluorophores are used to allow detection of multiple antigens on each slide using primary antibodies that may be raised in the same species. Sections were mounted in Prolong Gold (Thermo Fisher Scientific, MA, USA) and imaged using a TSC SP8 confocal microscope (Leica, Wetzlar, Germany). Images were processed using LAS X software (Leica), and Adobe Photoshop CS3 (Adobe Systems, CA, USA) was used to superimpose multiple color images. The antibodies used for immunofluorescence are summarized in **Table 1**.

Proximity ligation *in situ* hybridization

All procedures for proximity ligation *in situ* hybridization are based on a recent study [24] using mouse frozen lung sections. Six probes

for *Tgfb1* were designed as described below. The target and common sequences are shown in lower and upper case letters, respectively: (1) mmHR5X-Tgfb1-1429: tgacgtcaa-aagacagccac-TTATACGTCGAGTTGAACGTCGTAACA; (2) mmHL5X-Tgfb1-1429: TAGCGCTAACAACTTACGTCGTTATG-tcaggcgtatcagtggggggt; (3) mmHR5X-Tgfb1-1707: gcagttcttctctgtggagc-TTATACGTCGAGTTGAACGTCGTAACA; (4) mmHL5X-Tgfb1-1707: TAGCGCTAACAACTTACGTCGTTATG-tgaagcaatagttggatcc; (5) mmHR5X-Tgfb1-949: ccagctccatgctgatggtc-TTATACGTCGAGTTGAACGTCGTAACA and (6) mmHL5X-Tgfb1-949: TAGCGCTAACAACTTACGTCGTTATG-tgcaggtggagagtccccgc.

Quantification of collagen fiber, elastic fiber, fibronectin (FN1), type 1 collagen, and type 3 collagen content in the mouse pleura

To quantify the collagen fibers, elastic fibers, and FN1 content in mouse pleura, 20 areas per mouse containing only pleural tissue were randomly selected and observed using Sirius Red-stained, Victoria Blue-stained, and IHC lung sections. Digital images were converted to 8-bit grayscale images and threshold values applied, and then images were generated us-

Metformin reduces pleural fibroelastosis

ing ImageJ™ accessed using the NIH website (<https://imagej.nih.gov/ij/docs/examples/stained-sections/index.html>). Positive pixels were defined as the number of pixels exceeding the threshold per unit length (200 μm) along the pleura.

To quantify the type 1 and type 3 collagen content deposited in the pleura, 20 randomly selected areas were imaged after Sirius Red staining under a BX53 microscope with True Color LED using polarized light to distinguish between type 1 (bright yellow to red) and type 3 collagen (green). Using the CellSens imaging software (Olympus) to analyze sample images, the collagen fiber areas were automatically selected using color information, and the ratio of type 1 to type 3 collagen was measured in a 200 μm area along the pleura.

Cell isolation and FACS analysis

To prepare a single-cell suspension from mouse lungs for FACS analysis, lung tissue was incubated in 200 U/mL of collagenase type 2 (Worthington, NJ, USA) and 100 U/mL DNase I (Worthington) in Dulbecco's PBS (Gibco, CA, USA) at 37°C for 30 min. Single cells were treated with PE-conjugated anti-platelet-derived growth factor receptor A (PDGFRA) antibody, FITC-conjugated anti-CD90 (Thy-1.2) antibody, APC-conjugated antibodies against lineage-specific cell surface markers including CD31 (vascular endothelial cells), CD45 (hematopoietic cells), CD146 (pericytes and smooth muscle cells), E-cadherin (epithelial cells), LYVE1 (lymphatic endothelial cells), and TER-119 (erythrocytes) (Table 1), and Sytox Red Dead Cell Stain (1:1,000) (Thermo Fisher Scientific) for 30 min on ice. Samples were centrifuged (200 \times g, 5 min) and rinsed twice in FACS buffer. Sorting and analysis were performed using a FACS Aria (BD Biosciences, CA, USA).

Mouse primary cell culture

For primary cell culture, 5,000 FACS-sorted CD90^{pos} (myo)fibroblasts in fibrotic pleura were seeded in six-well plates and cultured overnight in Dulbecco's modified Eagle medium (DMEM; Gibco) supplemented with Glutamax (Gibco), 120 $\mu\text{g}/\text{mL}$ penicillin, 100 $\mu\text{g}/\text{mL}$ streptomycin, and 10% heat-inactivated fetal calf serum (Gibco) at 37°C in 20% O₂ and 5% CO₂. The next day, the medium was changed

into DMEM with 3% serum for 3 h, and then metformin (5 mM; Sumitomo Dainippon Pharma) was added and the (myo)fibroblasts were cultured for another 24 h.

Human tissue samples

We retrieved samples from four human lung autopsies (two normal cases; two cases of apical cap showing pleural fibrosis near bulla and that near lung adenocarcinoma), three cases of IPF, and three cases of idiopathic PPFE with surgical resection from the archives of the Hamamatsu University School of Medicine Hospital. Sequential 4 μm sections were prepared from the paraffin-embedded human lung samples for H&E staining, EVG staining, and IHC. IHC analyses were performed as described above using anti- α -smooth muscle actin (α SMA) and anti-CD90 antibodies after antigen retrieval.

Culture of MeT-5A cells and treatments

MeT-5A cells (human pleural mesothelial cells) were purchased from the American Type Culture Collection (VA, USA) and maintained in a basic medium (Medium 199 [Invitrogen], 10 ng/mL epidermal growth factor, 400 nM hydrocortisone, 870 mM insulin, 0.3% Trace Elements B [Mediatech, VA, USA], 120 $\mu\text{g}/\text{mL}$ penicillin, and 100 $\mu\text{g}/\text{mL}$ streptomycin) with 10% heat-inactivated fetal calf serum at 37°C in 20% O₂ and 5% CO₂. The cells were subcultured at a ratio of 1:3 once the cells had achieved approximately 80% confluence, and the culture medium was changed every 2 days. After four passages, the cells were cultured in basic medium with 3% serum with or without recombinant human transforming growth factor β 1 (TGF β 1) (10 ng/mL; PeproTech, NJ, USA) for 48 h and then treated with metformin (5 mM; Sumitomo Dainippon Pharma) for an additional 24 h.

Quantitative polymerase chain reaction (qPCR)

Total RNA was extracted from primary cultured cells, immortalized human mesothelial cells (MeT-5A), and 5,000 freshly isolated cells using TRIzol (Thermo Fisher Scientific) with glycogen as a carrier according to the manufacturer's instructions. The details of the qPCR procedure have been described previously [21-23]. The glyceraldehyde-3-phosphate dehydro-

Metformin reduces pleural fibroelastosis

Table 2. Primers used for quantitative PCR used in this study

Gene	Forward primer (5'-3')	Reverse primer (5'-3')
Mouse		
Glyceraldehyde-3-phosphate dehydrogenase (<i>Gapdh</i>)	AAC TTTGGCATTGTGGAAGG	GGATGCAGGGATGATGTTCT
Actin, alpha 2, smooth muscle, aorta (<i>Acta2</i>)	TGTGCTGGACTCTGGAGATG	GAAGGAATAGCCACGCTCAG
Collagen type 1 alpha 1 chain (<i>Col1a1</i>)	GAGCGGAGAGTACTGGATCG	GTTCCGGGCTGATGTACCAGT
Collagen type 3 alpha 1 chain (<i>Col3a1</i>)	GTCCACGAGGTGACAAAGGT	GATGCCCACTTGTCCATCT
Fibronectin 1 (<i>Fn1</i>)	AATGGAAGGGGAATGGAC	CTCGGTTGTCCTTCTTGCTC
Elastin (<i>Eln</i>)	GCTGATCCTCTTGCTCAACC	CAATACCAGCCCTGGATAA
Human		
Glyceraldehyde-3-phosphate dehydrogenase (<i>GAPDH</i>)	CGACCACTTTGTCAAGCTCA	AGGGGTCTACATGGCAACTG
Actin, alpha 2, smooth muscle, aorta (<i>ACTA2</i>)	TTCAATGTCCCAGCCATGTA	GAAGGAATAGCCACGCTCAG
Collagen type 1 alpha 1 chain (<i>COL1A1</i>)	GTGCTAAAGGTGCCAATGGT	CTCCTCGCTTTCTTCTCTCT
Collagen type 3 alpha 1 chain (<i>COL3A1</i>)	TACGGCAATCCTGAACTTCC	GTGTGTTTCGTGCAACCATC
Fibronectin 1 (<i>FN1</i>)	ACCAACCTACGGATGACTCG	GCTCATCATCTGGCCATTTT
Elastin (<i>ELN</i>)	GGTGGCTTAGGAGTGTCTGC	CCAGCAAAAGCTCCACCTAC
Snail family zinc finger 1 (<i>SNAI1</i>)	ACCCACATCCTTCTCACTG	TACAAAAACCCACGCAGACA

genase (GAPDH) gene was used as an internal control both mouse and humans. The primer sequences are listed in **Table 2**.

Re-analysis of single-cell RNAseq dataset

A published single-cell RNAseq dataset (GSM-3688759) [25], including CD45-negative live cells isolated from C57BL/6 female mice aged 6 to 8 weeks old, was re-analyzed. Using the Seurat R package, 'Uniform Manifold Approximation and Projection (UMAP) plot' and 'dot plot' were drawn.

Statistics

All results are presented as mean \pm standard deviation from a minimum of three independent experiments. Statistical analyses were performed using unpaired Student's t-test (two-tailed) for comparisons between two groups or one-way analysis of variance with Bonferroni correction for comparisons between more than two groups. Differences with $P < 0.05$ were considered significant.

Study approval

All animal and human research in this study was performed after approval by the local research ethics committees at the Hamamatsu University School of Medicine. The Animal Care and Use Committee of Hamamatsu University School of Medicine (approval num-

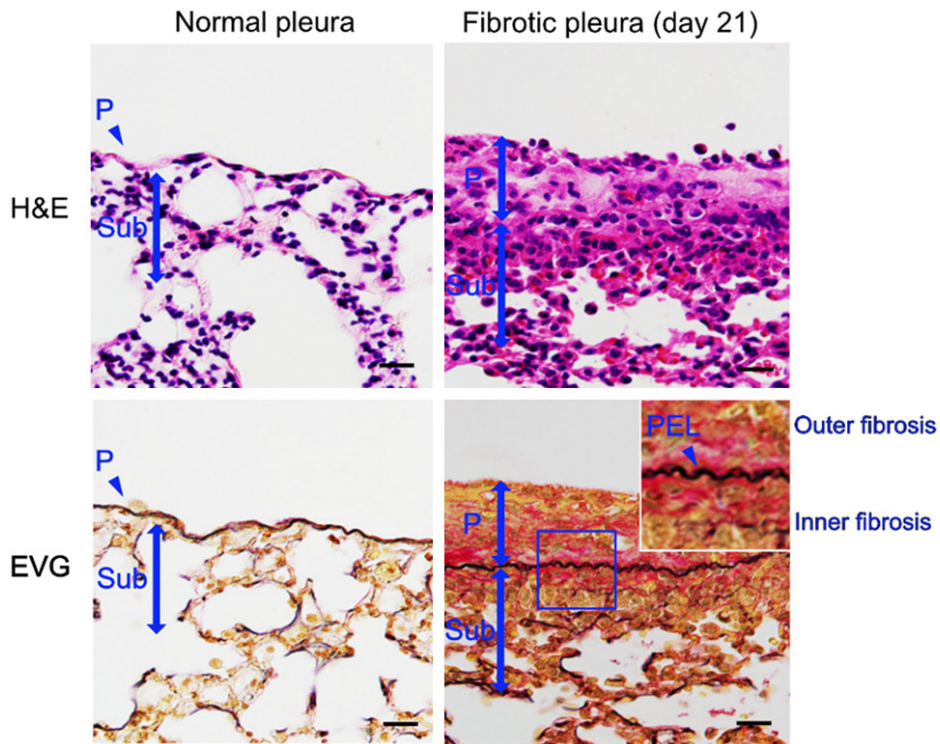
ber: 2018015) approved all animal experiments and procedures, which complied with the ARRIVE guidelines and were carried out in accordance with the National Institutes of Health Guide for the Care and Use of Laboratory Animals. With respect to the use and collection of human tissue samples, all patients provided written informed consent for the use of their tissue samples, and the study was approved by the Institutional Review Board of Hamamatsu University School of Medicine (approval number: 14-365).

Results

Histologic comparison of mouse pleural fibrosis model with human pleural fibrosis

The mouse model of pleural fibrosis was generated using intra-pleural coadministration of bleomycin and carbon (**Figure 1A**). Compared to normal pleura, the pleural fibrosis model pleura showed considerable collagen deposition on the outer side of the elastic layer, elastic fibers separating the pleura from the lung parenchyma, and a small quantity of collagen deposition on the inner (parenchymal) side. Pleural fibrosis in the mouse model had similar collagen fiber deposition to human pleural fibrosis (including PPFE), particularly outside the pleural elastic layer (**Figure 1B**). However, while some of the fibrotic pleura in the mouse model showed severe fibroelastosis (**Figure 2**), it was difficult to reproduce the 'intra-alveolar

A Mouse lungs



B Human lungs

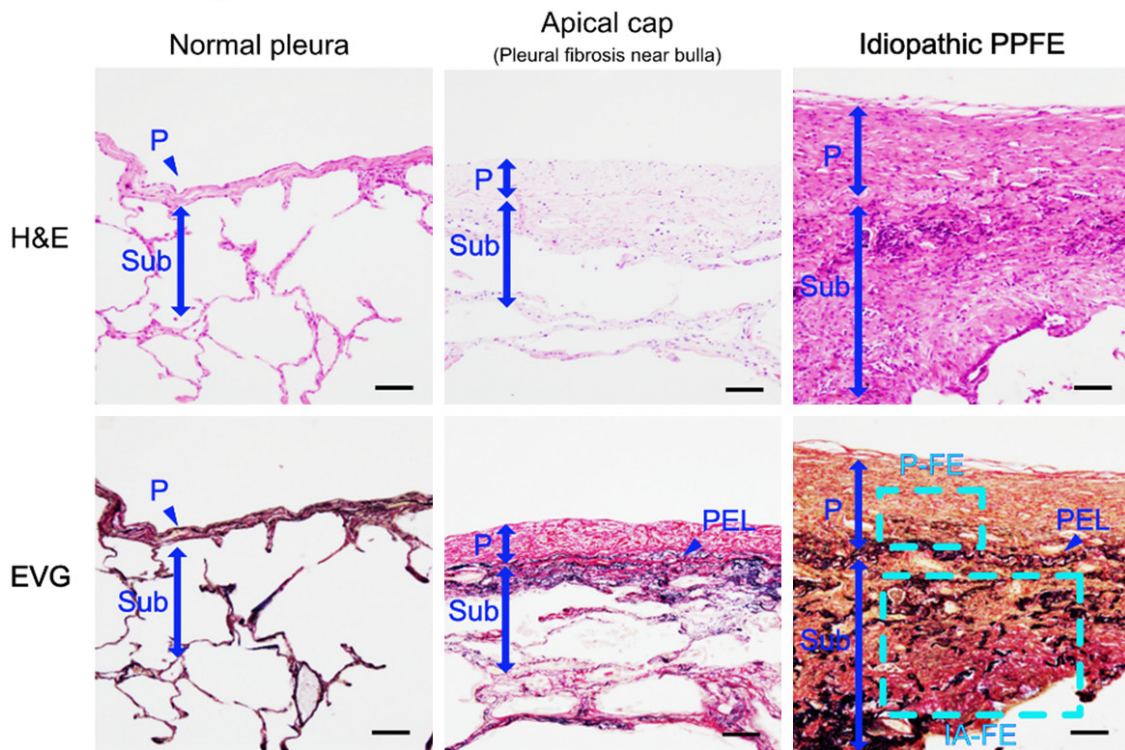


Figure 1. Hematoxylin & eosin (H&E) and Elastica van Gieson (EVG) staining of the pleural/subpleural areas of mouse and human lungs. A. Control untreated mouse lung and mouse lung with pleural fibrosis on day 21 after intra-pleural coadministration of bleomycin and carbon. Scale bars: 20 μ m (\times 400). B. Control normal human lung,

Metformin reduces pleural fibroelastosis

lung of apical cap (pleural fibrosis near bulla), and lung of idiopathic pleuroparenchymal fibroelastosis (PPFE). Scale bar: 100 μm ($\times 100$). In EVG staining, collagen fibers are indicated as red bundles, and elastic fibers are indicated as black bundles. P, pleura; Sub, subpleural area; PEL, pleural elastic layer; P-FE, pleural fibroelastosis; IA-FE, intra-alveolar fibroelastosis.

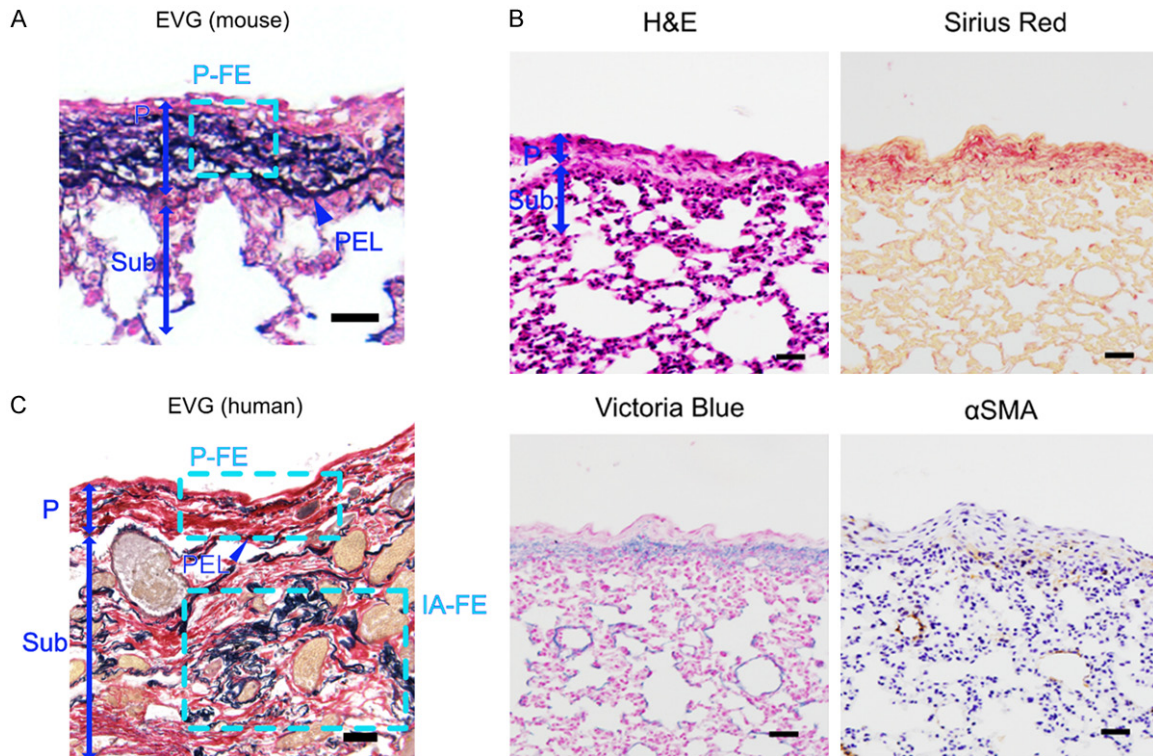


Figure 2. Mouse and human lungs with pleural fibroelastosis. A, B. Mouse lung from a pleural fibrosis model (day 21). A. EVG staining. P, pleura; Sub, subpleural area; PEL, pleural elastic layer; P-FE, pleural fibroelastosis. Scale bar: 20 μm ($\times 100$). B. Serial sections: H&E staining; Sirius Red staining (collagen fibres indicated as red bundles); Victoria Blue staining (elastic fibres indicated as blue bundles); immunohistochemistry using anti- αSMA antibody. P, pleura; Sub, subpleural area. Scale bars: 50 μm ($\times 200$). C. EVG staining of human lung from a patient with idiopathic pleuroparenchymal fibroelastosis. P, pleura; Sub, subpleural area; PEL, pleural elastic layer; P-FE, pleural fibroelastosis; IA-FE, intra-alveolar fibroelastosis. Scale bar: 50 μm ($\times 100$).

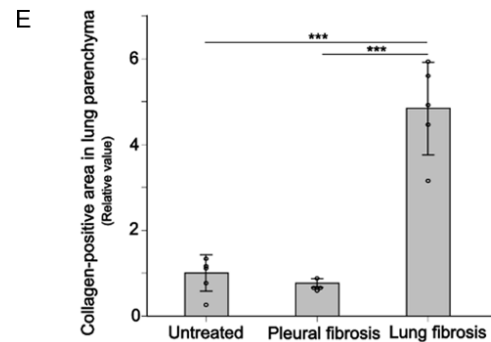
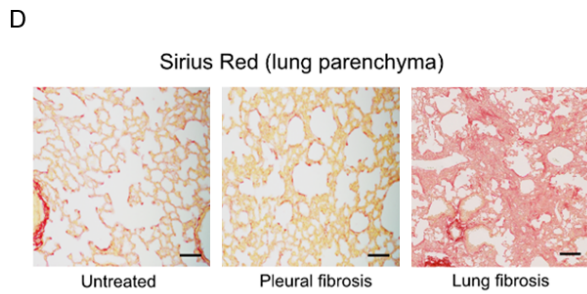
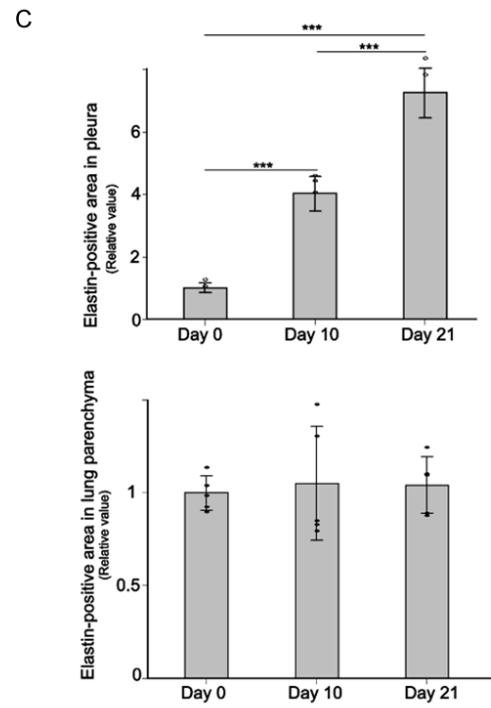
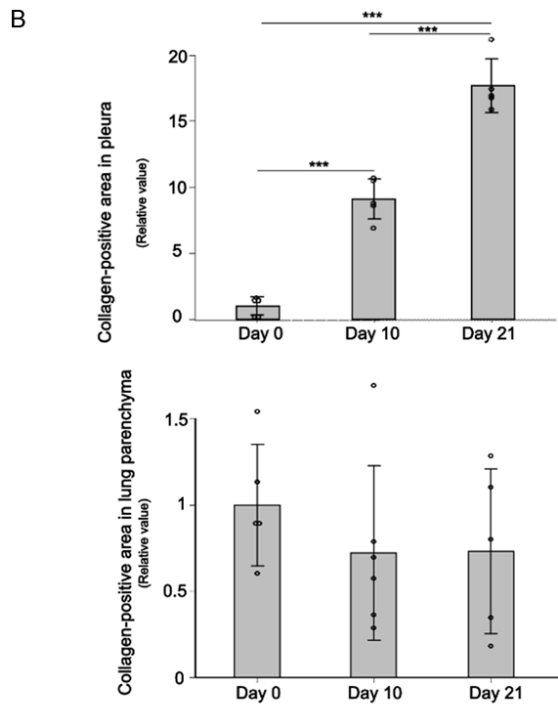
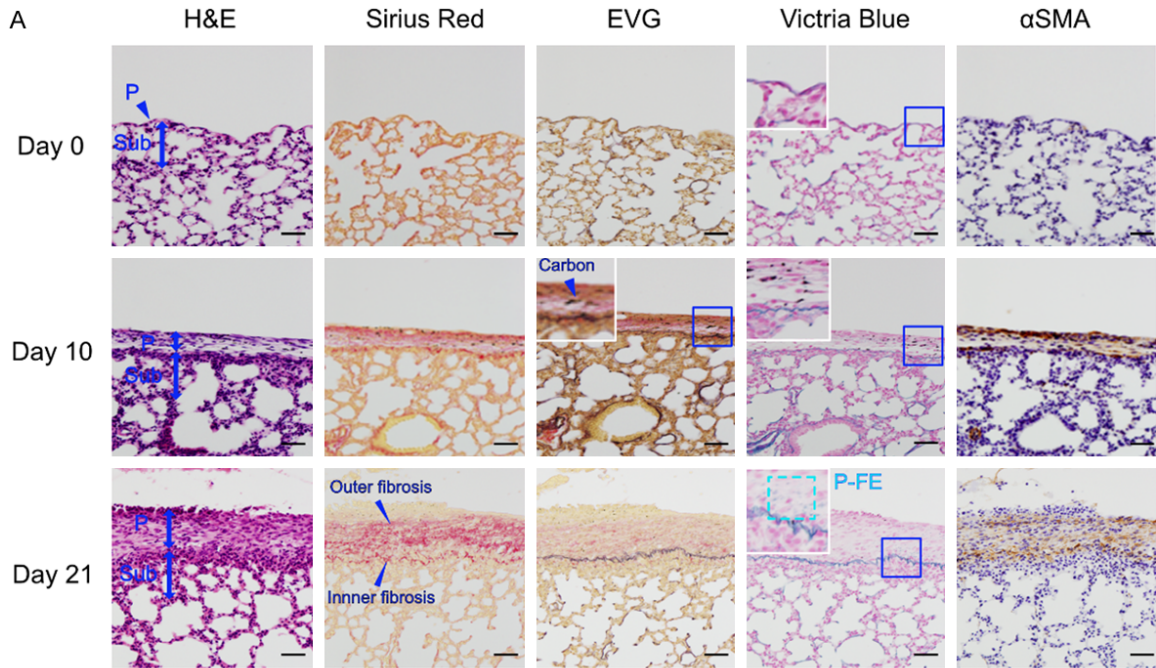
fibroelastosis' often seen in PPFE lungs in the subpleural area.

Characterization of the mouse pleural fibrosis model

The presence of collagen fiber deposition in the fibrotic pleura was confirmed by Sirius Red staining and elastic fiber deposition by EVG staining (black coloration) and Victoria Blue staining (blue coloration). In addition, myofibroblasts in the fibrotic pleura were identified by immunostaining of αSMA (Figure 3A). On day 10 after coadministration of bleomycin and carbon, EVG and Victoria Blue staining revealed a clear pleural elastic layer and Sirius Red staining showed deposition of collagen fibers on the outer and inner sides of the pleural

elastic layer. Compared to day 10, significantly more accumulation of collagen and elastic fibers was observed in the pleura on day 21. In contrast, in the lung parenchyma away from the pleura, there was no difference in collagen and elastic fiber content between the treated and untreated lungs (Figure 3B and 3C). αSMA -positive myofibroblasts appeared by day 10 and gradually increased by day 21, although the intensity of αSMA expression appeared to decrease in a time-dependent manner (Figure 3A). The lung parenchyma of mice administered intra-pleural bleomycin with carbon (pleural fibrosis model) exhibited negligible signs of parenchymal fibrosis, unlike that of mice administered intratracheal bleomycin (lung fibrosis model) (Figure 3D and 3E).

Metformin reduces pleural fibroelastosis



Metformin reduces pleural fibroelastosis

Figure 3. Collagen and elastic fibers in mouse lungs of pleural fibrosis model. (A) Serial sections of the pleural/subpleural areas of murine lungs with pleural fibrosis on days 0, 10 and 21: H&E staining; Sirius Red staining (collagen fibres indicated as red bundles); EVG staining (elastic fibres indicated as black bundles); Victoria Blue staining (elastic fibres indicated as blue bundles); immunohistochemistry using anti- α SMA antibody. P, pleura; Sub, subpleural area; P-FE, pleural fibroelastosis. Scale bars: 50 μ m (\times 200). (B, C) Quantification of (B) collagen fibers (Sirius Red staining) and (C) of elastic fibers (Victoria Blue staining) deposited on the pleura (upper panels) and non-pleural/subpleural lung parenchyma (lower panels) of lungs with pleural fibrosis on days 0, 10 and 21. Data represent mean values \pm standard deviations of the results obtained from five independent experiments (mice) performed in triplicate. Statistical analyses were performed using one-way analysis of variance with Bonferroni correction. *** $P < 0.001$. (D) Sirius Red staining of the non-pleural/subpleural lung parenchyma: untreated case; pleural fibrosis model on day 21; and lung fibrosis model on day 21. Scale bars: 100 μ m (\times 100). (E) Quantification of collagen fibers in the lung parenchyma. Data represent mean values \pm standard deviations of the results obtained from five independent experiments performed in triplicate. Statistical analyses were performed using one-way analyses of variance with Bonferroni correction. *** $P < 0.001$.

Identification of a cell surface marker for (myo) fibroblasts in the mouse fibrotic pleura

Using IHC, we found that $\text{lin}^{\text{neg}}\text{PDGFRA}^{\text{pos}}$ (myo) fibroblasts were increased in the fibrotic pleura (**Figure 4A**). However, as normal/fibrotic lung parenchymal fibroblasts/myofibroblasts both express $\text{lin}^{\text{neg}}\text{PDGFRA}^{\text{pos}}$ [22-24], we sought to distinguish them by evaluating the expression levels of three candidate surface markers in the $\text{lin}^{\text{neg}}\text{PDGFRA}^{\text{pos}}$ cells (CD34, PDGFRB, and CD90) that could be positive in mesenchymal cells including (myo)fibroblasts. In the $\text{lin}^{\text{neg}}\text{PDGFRA}^{\text{pos}}$ (myo)fibroblasts from lungs of the pleural fibrosis model, only CD90 expression was significantly and specifically high (**Figure 4B**).

In our re-analysis of a published single-cell RNAseq dataset from normal adult mouse lungs [25], we found that the gene expression of CD90 (*Thy1*) was commonly low among non-hematopoietic cells, including in pleural mesothelial cells and fibroblasts (**Figure 4C**). Consistent with this finding, we were unable to detect CD90^{pos} cells in the pleura/subpleura of normal lungs by immunofluorescence staining. In contrast, CD90^{pos} cells were increased in the fibrotic pleura of the mouse model (**Figure 4D**).

Next, to confirm whether bleomycin affects CD90 expression in lung parenchymal fibroblasts, we measured CD90 expression in lung parenchymal (myo)fibroblasts from the lung fibrosis model using FACS. The number of $\text{lin}^{\text{neg}}\text{PDGFRA}^{\text{pos}}\text{CD90}^{\text{pos}}$ (myo)fibroblasts in the lung fibrosis model did not significantly differ from that in normal control lungs (**Figure 4E**), suggesting that intratracheal bleomycin treatment did not upregulate CD90 expression in lung parenchymal (myo)fibroblasts.

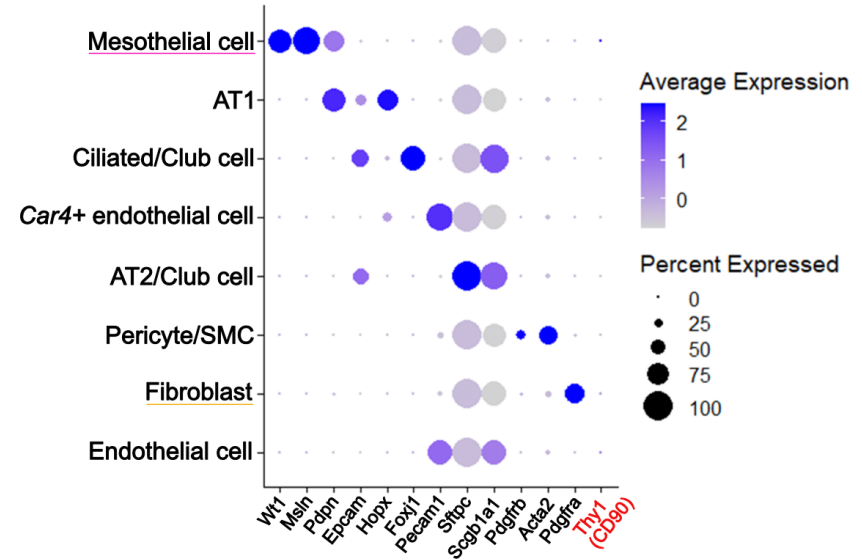
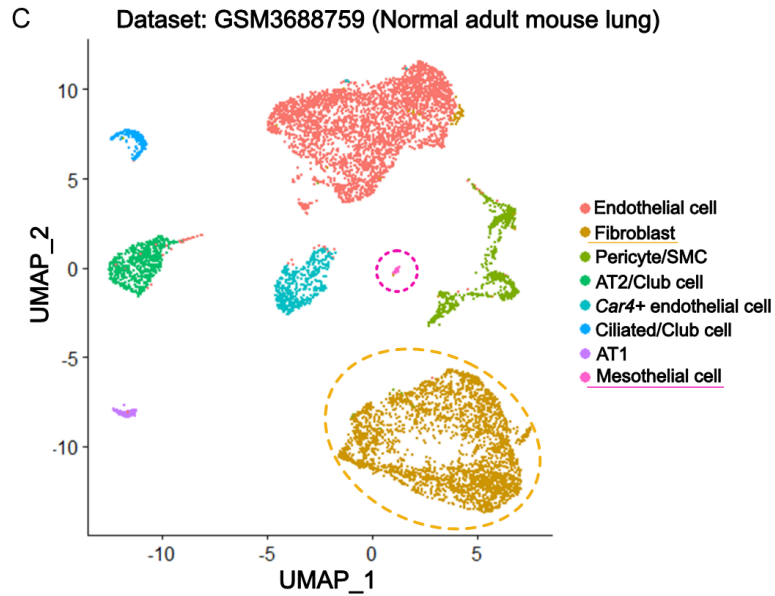
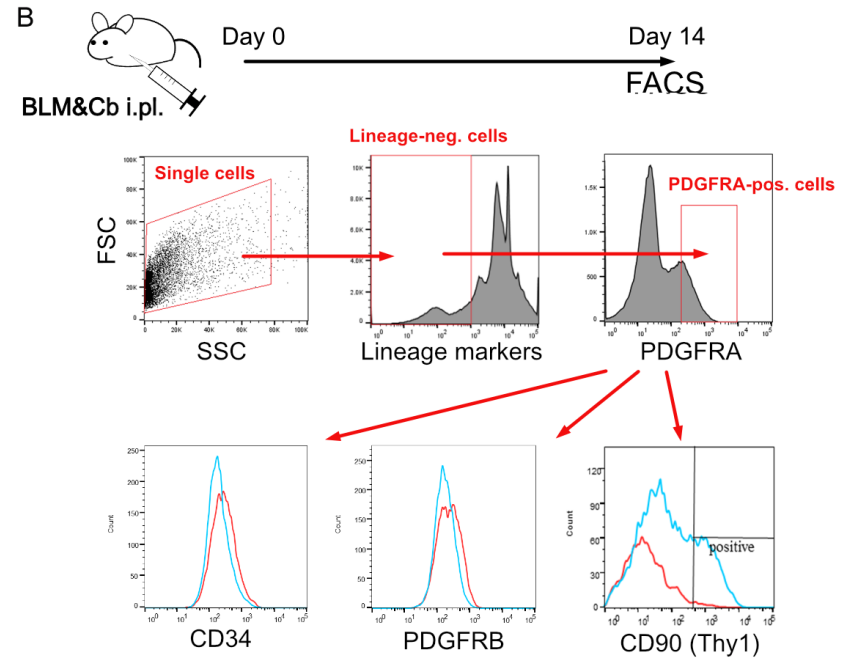
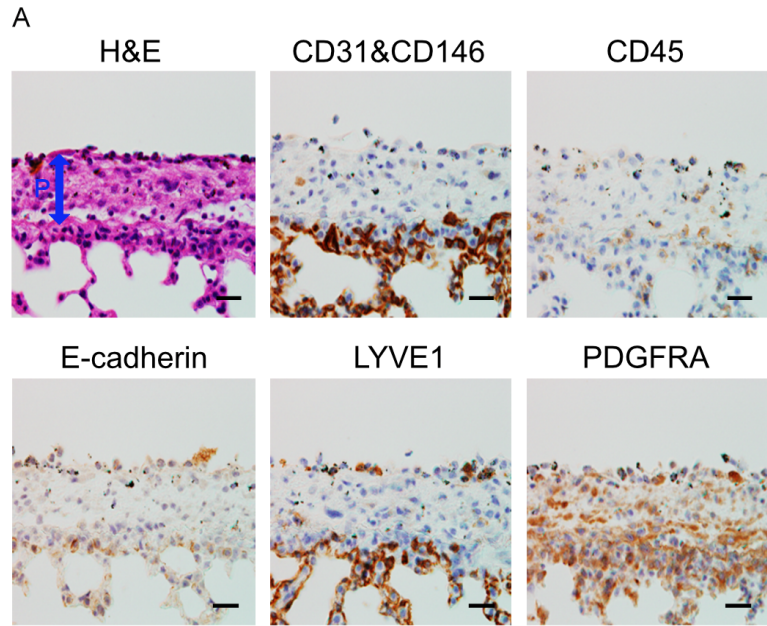
Collectively, these results indicate that CD90 is a specific cell surface marker able to distinguish between (myo)fibroblasts from the fibrotic pleura and the lung parenchyma.

Profiling of CD90^{pos} (myo)fibroblasts in the mouse fibrotic pleura

In our high-magnification immunostaining of the fibrotic pleura, we found that CD90 co-stained primarily with α SMA and rarely with CD3 (a T-cell marker), indicating that CD90^{pos} CD3^{neg} cells are *bona fide* myofibroblasts in this model (**Figure 5A**). In addition, these myofibroblasts commonly expressed phosphorylated SMAD2/3 in the nuclei (**Figure 5B**), suggesting that the TGF β 1-SMAD pathway is activated. This pathway plays a significant role in organ fibrosis. In our *in situ* hybridization experiment, the expression of *Tgfb1* mRNA was highly increased in CD3^{neg} α SMA^{pos} (myo)fibroblasts in the fibrotic pleura, whereas lung parenchymal upregulation of *Tgfb1* was not apparent compared to untreated control lungs (**Figure 5C**). These results suggest that CD90^{pos} (myo)fibroblasts may represent one of the sources of TGF- β 1, and autocrine signaling might therefore enhance the fibrotic process.

In quantitative RT-PCR (**Figure 5D**), the expression levels of genes encoding α SMA (*Acta2*) and elastin (*Eln*) were significantly higher in the CD90^{pos} (myo)fibroblasts than in normal lung parenchymal $\text{lin}^{\text{neg}}\text{PDGFRA}^{\text{pos}}$ fibroblasts, consistent with the staining results in **Figure 3A**. In addition, major ECM components, such as collagen 1 α 1 (*Col1a1*), collagen 3 α 1 (*Col3a1*) and fibronectin (*Fn1*), were commonly upregulated in the CD90^{pos} (myo)fibroblasts. To further confirm the upregulation of these ECM components at the protein level, we added Sirius Red

Metformin reduces pleural fibroelastosis



Metformin reduces pleural fibroelastosis

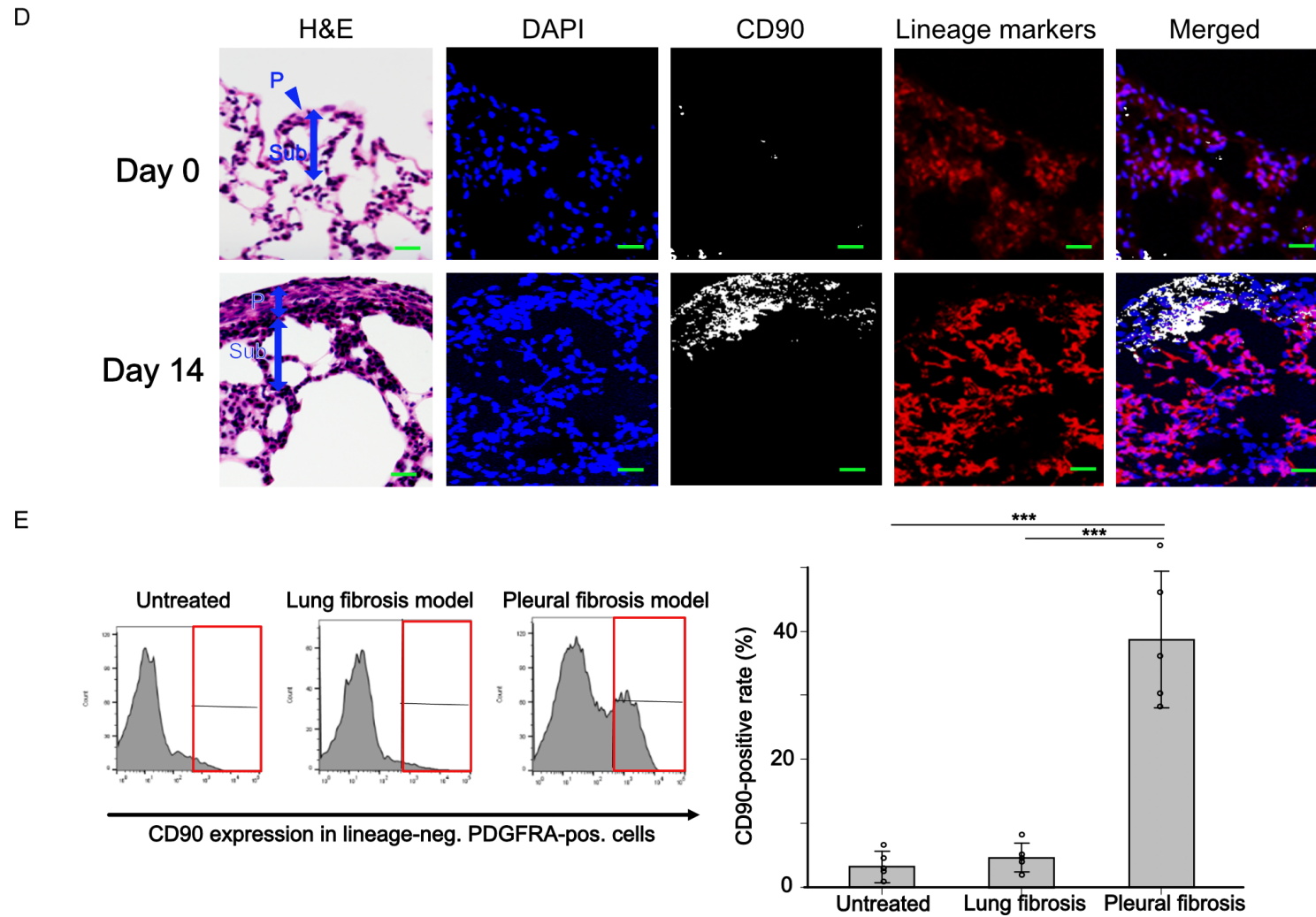


Figure 4. Identification of a cell surface marker for (myo)fibroblasts located in the mouse fibrotic pleura. A. Serial sections of the pleural and subpleural areas of lungs with pleural fibrosis on day 14: H&E staining; immunohistochemistry using antibodies against CD31&CD146, CD45, E-cadherin, LYVE1, and PDGFRA. P, pleura. Scale bars: 20 μ m (\times 400). B. FACS panels of the (myo)fibroblasts. Positivity for CD34, PDGFRB or CD90 was evaluated within lineage-negative and PDGFRA-positive single cells. In the lower panels, the red lines show data from control untreated lungs and the blue lines indicate data from lungs with pleural fibrosis on day 14. C. Re-analysis of a single-cell RNAseq dataset from adult wild-type mouse lungs: Uniform Manifold Approximation and Projection (UMAP) plot (left) and dot plot (right). AT1/2, alveolar epithelial cell type 1/2; SMC, smooth muscle cell. D. Localization of CD90^{pos} (myo)fibroblasts in lungs with pleural fibrosis on day 14: H&E staining; DAPI staining (blue); immunofluorescence using anti-CD90 antibody (white); a mixture of antibodies against lineage markers (CD31, CD45, CD146, E-cadherin, LYVE1, and TER-119) (red) and merged images. P, pleura; Sub, subpleural area. Scale bars: 50 μ m (\times 200). E. FACS panels using anti-CD90 antibody

Metformin reduces pleural fibroelastosis

and the quantification between control untreated lung, lung with parenchymal fibrosis induced by an intratracheal administration of bleomycin (lung fibrosis model on day 21), and lung with pleural fibrosis induced by an intrapleural coadministration of bleomycin and carbon (pleural fibrosis model on day 21). Data represent mean values \pm standard deviations of results obtained from five independent experiments (mice) performed in triplicate. Statistical analyses were performed using one-way analyses of variance with Bonferroni correction. *** $P < 0.001$.

staining with polarised light, which distinguishes between type 1 and 3 collagen fibers, and performed immunostaining for FN1. As expected, the fibrotic pleura, which includes abundant CD90^{pos} (myo)fibroblasts, showed high levels of type 1 and 3 collagen fibers and FN1 deposition (**Figure 5E** and **5F**). Collectively, CD90^{pos} (myo)fibroblasts in the fibrotic pleura produced excessive ECM proteins, which would have led to pleural fibroelastosis.

Effects of metformin on pleural fibrosis and elastosis in vivo

To investigate the anti-fibrotic effects of metformin on pleural fibroelastosis, pleural fibrosis model mice were further treated with intra-peritoneal administration of metformin (62.5 mg/kg) or PBS (as a control) every other day from day 10 to day 21. The metformin-treated mice had reduced thickness of fibrotic pleura compared to the PBS-treated mice (**Figure 6A**). Moreover, type 1 and 3 collagen fiber deposition, FN1 expression, and elastic fiber deposition were significantly reduced in the metformin-treated mice, suggesting that metformin suppressed pleural fibroelastosis *in vivo* (**Figure 6A** and **6B**).

Effects of metformin on CD90^{pos} (myo)fibroblasts in the mouse fibrotic pleura

Next, we evaluated the effects of metformin at a cellular/molecular level. The number of CD90^{pos} (myo)fibroblasts in the metformin-treated mice was significantly decreased compared to that in the PBS-treated mice (mean: 19.5% vs. 30.1%, $P < 0.05$; **Figure 6C**). Gene expression levels of *Acta2* (α SMA), *Col1a1*, *Col3a1*, *Fn1*, and *Eln* in the CD90^{pos} (myo)fibroblasts isolated from metformin-treated mice were decreased compared to those isolated from the PBS-treated mice (**Figure 6D**). To further study the effects of metformin following (myo)fibroblast formation, the mRNA expression of genes related to the ECM was analyzed in primary cultured CD90^{pos} (myo)fibroblasts in the presence or absence of metformin. Metformin significantly downregulated the ex-

pression of *Col1a1* and *Eln* mRNA (**Figure 6E**). These results suggest that metformin suppresses not only proliferation of CD90^{pos} (myo)fibroblasts but also ECM production by these cells.

CD90 expression in human pleura/subpleura and the effects of metformin on TGF β 1-treated human pleural mesothelial cells in vitro

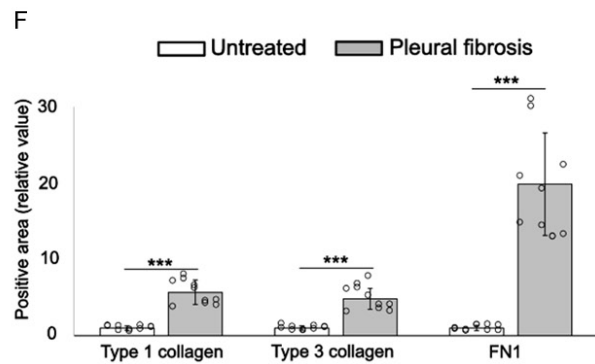
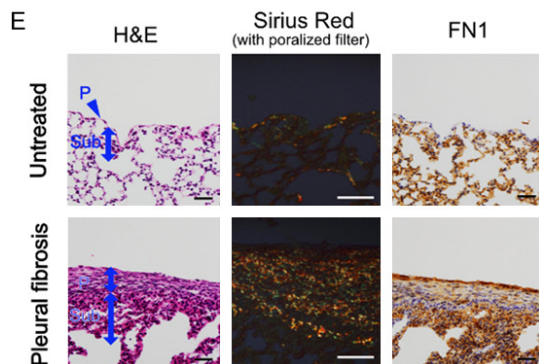
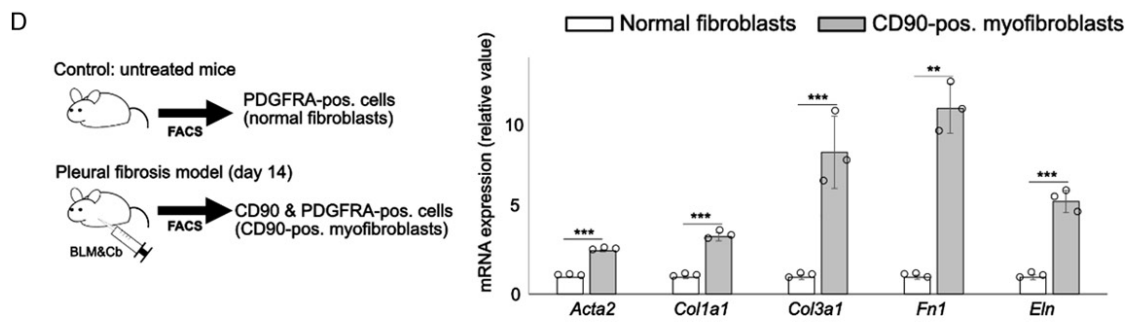
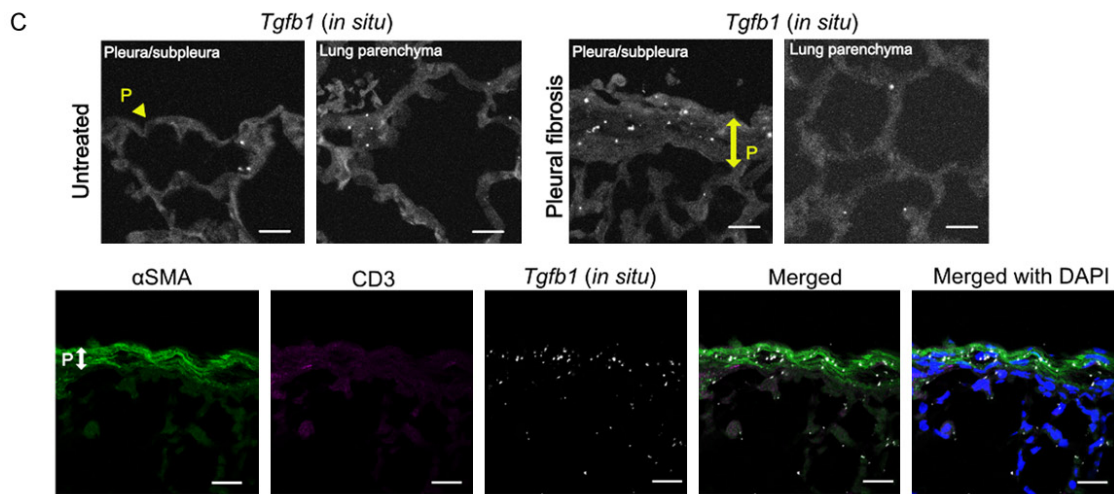
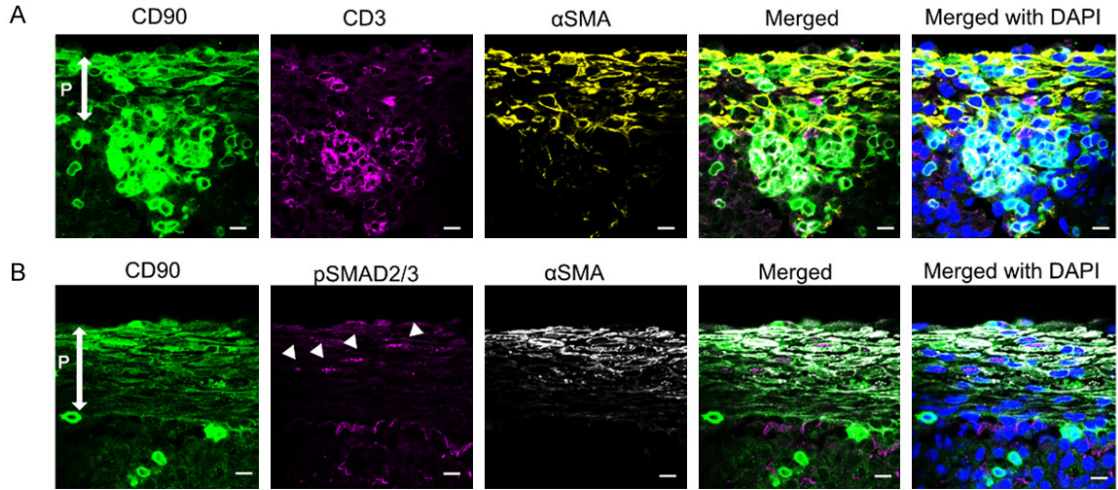
Next, we sought to investigate whether CD90 is also expressed in pleural/subpleural (myo)fibroblasts and/or mesothelial cells in human lungs. CD90^{pos} cells were not detected in the pleura/subpleura of normal lungs nor in the lungs of patients with IPF (**Figure 7A**). However, samples collected from the apical cap and from PPF commonly contained CD90^{pos} (myo)fibroblasts co-expressing α SMA, suggesting that the increase in CD90^{pos} (myo)fibroblasts in the fibrotic pleura is a finding common to both mice and humans.

When mesothelial cells are stimulated by TGF β , they can acquire a (myo)fibroblast-like phenotype, a process termed mesothelial-to-mesenchymal transition (MMT), leading to secretion of excessive ECM proteins and pleural fibrosis [20, 26]. Therefore, we investigated the effect of metformin on TGF β 1-induced MMT in human mesothelial cells (MeT-5A cells). When the cells were stimulated with TGF β 1 (10 ng/mL), they differentiated into cells with more mesenchymal characteristics, including increased expression of ECM-related genes and the major MMT marker *SNAI1* (**Figure 7B**). Interestingly, metformin significantly reduced the expression levels of *COL1A1*, *COL3A1*, and *SNAI1*, but did not affect those of *FN1* and *ELN*. These results indicate that metformin suppressed TGF β 1-induced MMT and TGF β 1-induced upregulation of genes encoding components of the ECM in human mesothelial cells.

Discussion

In this study, using a mouse pleural fibrosis model, we identified CD90 as a novel cell surface marker of pleural (myo)fibroblasts and

Metformin reduces pleural fibroelastosis



Metformin reduces pleural fibroelastosis

Figure 5. Profiling of CD90^{pos} (myo)fibroblasts located in the mouse fibrotic pleura. A. High magnification images of fibrotic pleura (day 10) showing CD90^{pos}CD3^{neg}αSMA^{pos} myofibroblasts: immunofluorescence using anti-CD90 antibody (green); anti-CD3 antibody (magenta); anti-αSMA antibody (yellow) and merged images with or without DAPI (blue). P, pleura. Scale bars: 10 μm (×630). B. High magnification images of fibrotic pleura (day 10) showing CD90^{pos}αSMA^{pos} myofibroblasts with nuclear expression of pSMAD2/3: immunofluorescence using anti-CD90 antibody (green); anti-pSMAD2/3 antibody (magenta); anti-αSMA antibody (white) and merged images with or without DAPI (blue). Triangles indicate pSMAD2/3-positive nuclei. P, pleura. Scale bars: 10 μm (×630). C. High magnification images of normal-untreated or fibrotic pleura (day 10) showing *Tgfb1*-mRNA expressions (white dots). Lower panels show the combination with immunofluorescence using anti-αSMA antibody (green); anti-CD3 antibody (magenta) and merged images with or without DAPI (blue). P, pleura. Scale bars: 20 μm (×630). D. Quantitative PCR using cDNA samples of lin^{neg}PDGFRA^{pos} cells isolated from the untreated control lungs (normal fibroblasts) and lin^{neg}PDGFRA^{pos}CD90^{pos} cells isolated from lungs with pleural fibrosis on day 14 (CD90-positive myofibroblasts). Data represent mean values ± standard deviations of the results obtained from three independent experiments (mice) performed in triplicate. Statistical analyses were performed using unpaired Student's t-tests (two-tailed). ***P*<0.01, ****P*<0.001. E. Serial sections of the pleural/subpleural areas of untreated control lungs and lungs with pleural fibrosis on day 21: H&E staining; Sirius Red staining with polarized light and immunohistochemistry using anti-FN1 antibody. P, pleura; Sub, subpleural area. Scale bars: 50 μm (×200). F. Quantification of type 1 and type 3 collagen fibers (by Sirius Red staining with polarised light) and FN1 (by immunostaining) in pleural tissues of the untreated control lungs and lungs with pleural fibrosis on day 21. Data represent mean values ± standard deviations of the results obtained from ten independent experiments (mice) performed in triplicate. Statistical analyses were performed using unpaired Student's t-tests (two-tailed). ****P*<0.001.

evaluated the characteristics of this model, providing insight into the pathogenesis of pleural fibrosis and elastosis. In addition, we were able to determine the effects of metformin at both an individual and cellular/molecular level, revealing that it significantly attenuated pleural fibroelastosis via suppression of ECM protein production from CD90^{pos} (myo)fibroblasts.

Relevant rodent preclinical models are vital to understand the pathogenesis of and identify effective treatments for intractable diseases and to facilitate *in vivo* studies. PPFE is a lethal disease with unknown etiology [3-9], but to our knowledge, no appropriate experimental models of PPFE have been reported. In this study, we used a mouse model in which the mouse fibrotic pleura had similar morphological features to that of human fibrotic pleura in PPFE lungs, with significant deposition of collagen and elastic fibers (pleural fibroelastosis, **Figures 1 and 2**). However, another hallmark of PPFE is intra-alveolar fibroelastosis, comprising prominent deposition of subpleural elastic fibers with frequent alveolar collapse, and this was not fully reproduced in the mouse model. A summary comparing the morphologic features and immunoreactivity of pleural myofibroblasts of the mouse pleural fibrosis model to human PPFE lungs [27] is given in **Table 3**. Although these differences must be taken into account, the similarity of the pleural features indicates that our model is relevant and our experimental findings can be translated into the study of PPFE.

Using this mouse model, we identified CD90 as a specific cell surface marker of pleural (myo) fibroblasts. In mice, CD90 (Thy-1) is expressed in various types of cells, including thymocytes, T cells, epidermal cells, keratinocytes, neural cells, lymphatic endothelial cells, and a small number of fibroblasts, but its precise function remains unclear. We could not clearly detect CD90^{pos} fibroblasts in normal mouse lungs in our previous [22] or present study. This differs from previous reports [28, 29] but appears consistent with the results of single-cell RNAseq re-analysis (**Figure 4C**). Our FACS analysis detected a minor population of CD90^{pos} fibroblasts in normal mouse lungs, which may be similar to those found near the hilar region by Kretschmer et al. [30].

The origin of the CD90^{pos} pleural (myo)fibroblasts remains unclear in our study. As fibrosis occurs almost uniformly throughout the pleura in the pleural fibrosis model, the hilar CD90^{pos} fibroblasts or lipid-rich alveolar fibroblasts [28, 29] are unlikely to serve as the primary sources of pleural CD90^{pos} (myo)fibroblasts. It is possible that the resident fibroblasts surrounding the pleura might acquire CD90 expression because mesothelial cells can recruit surrounding fibroblasts using fibronectin as a chemoattractant [31]. However, based on consistent results from previous studies using experimental pleural fibrosis models [20, 26, 32], it is more likely that mesothelial cells present in the injured visceral pleura undergo MMT and differentiate into myofibroblasts. Interestingly,

Metformin reduces pleural fibroelastosis

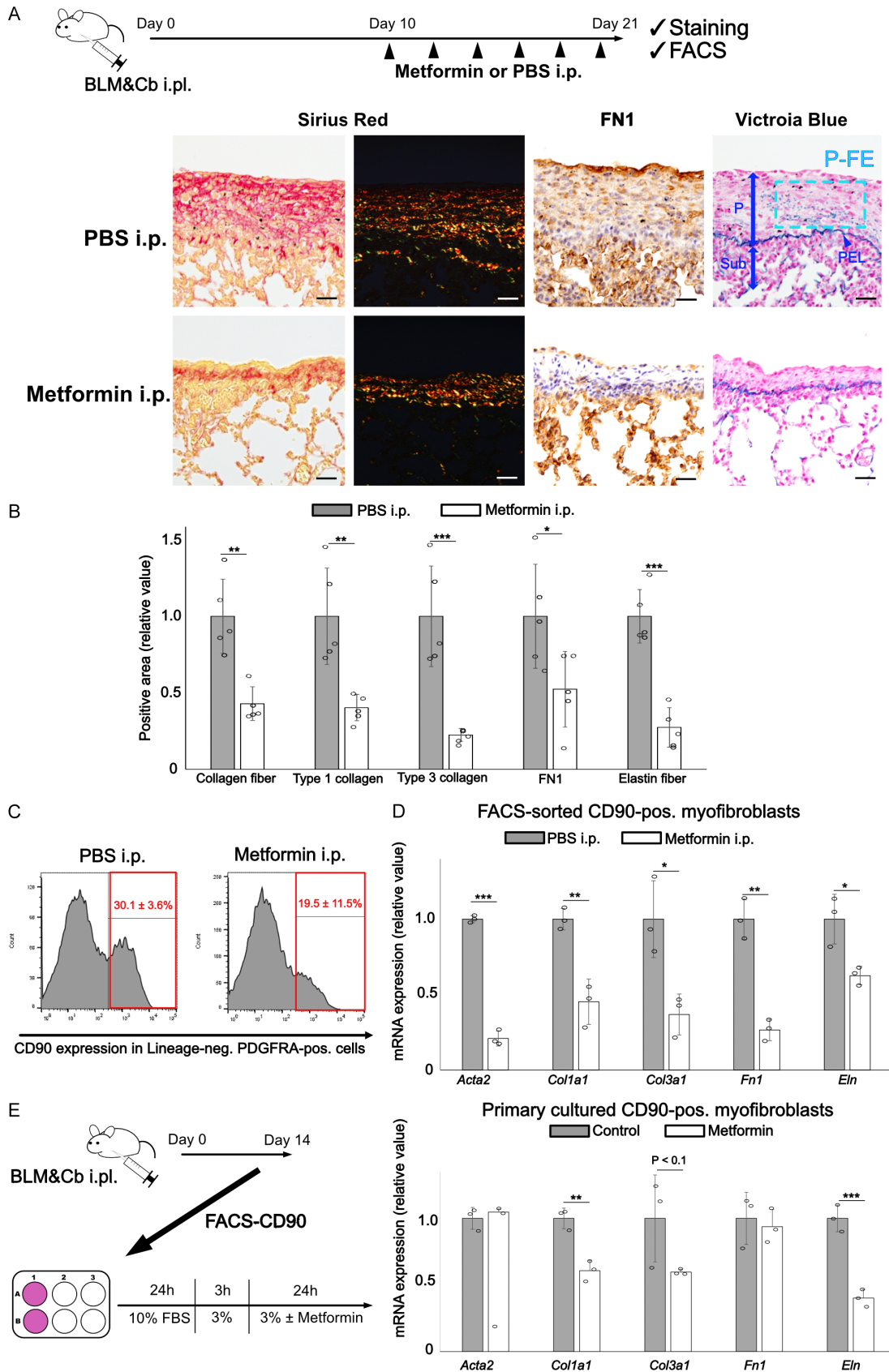
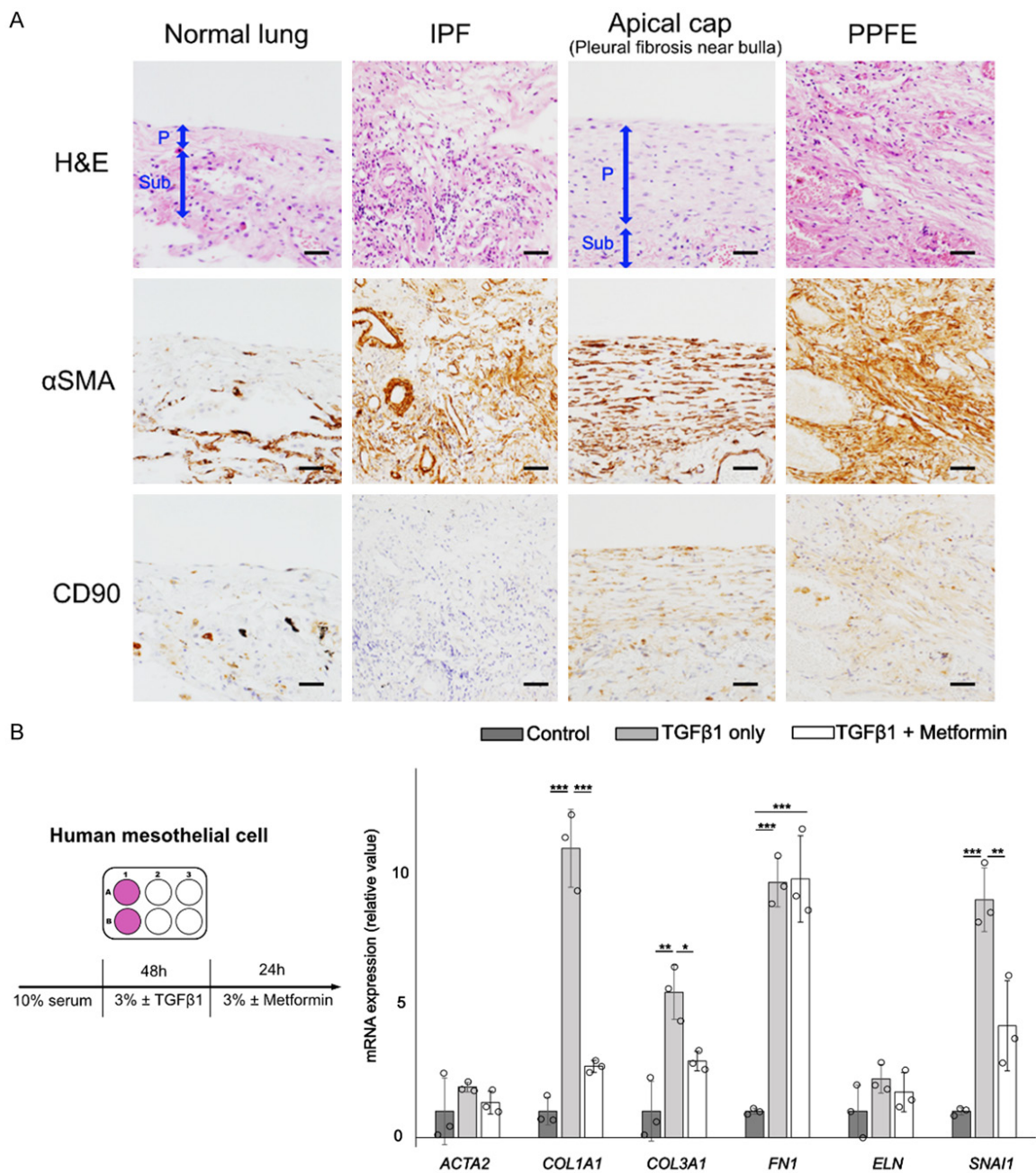


Figure 6. Effects of metformin on pleural fibroelastosis and CD90^{pos} (myo)fibroblasts located in the mouse fibrotic pleura. A. Serial sections of lungs with pleural fibrosis treated by intra-peritoneal metformin or PBS; H&E staining;

Metformin reduces pleural fibroelastosis

Sirius Red staining with bright field; Sirius Red staining with polarized light; immunohistochemistry using anti-FN1 antibody; Victoria Blue staining. P, pleura; Sub, subpleural area; PEL, pleural elastic layer; P-FE, pleural fibroelastosis. Scale bars: 50 μm ($\times 200$). B. Quantification of collagen fibers using Sirius Red staining with bright-field microscopy, type 1 and 3 collagen fibers using Sirius Red staining with a polarised filter and FN1 expression using immunostaining and elastic fibers using Victoria Blue staining. Data represent mean values \pm standard deviations of results obtained from five independent experiments (mice) performed in triplicate. Statistical analyses were performed using unpaired Student's t-tests (two-tailed). $**P < 0.01$, $***P < 0.001$. C. FACS panels and their quantification showing the expression of CD90 in $\text{lin}^{\text{neg}}\text{PDGFR}\alpha^{\text{pos}}$ cells derived from lungs with pleural fibrosis. Data represent mean values \pm standard deviations of results obtained from six mice each. D. Quantitative PCR using cDNA samples of CD90^{pos} (myo)fibroblasts isolated from PBS- or metformin-treated lungs with pleural fibrosis. Data represent mean values \pm standard deviations of the results obtained from three independent experiments (mice) performed in triplicate. Statistical analyses were performed using unpaired Student's t-tests (two-tailed). $*P < 0.05$, $**P < 0.01$, $***P < 0.001$. E. Quantitative PCR using cDNA samples of primary cultured CD90^{pos} (myo)fibroblasts in the absence or presence of metformin. Data represent mean values \pm standard deviations of the results obtained from three independent experiments (mice) performed in triplicate. Statistical analyses were performed using unpaired Student's t-tests (two-tailed). $**P < 0.01$, $***P < 0.001$.



Metformin reduces pleural fibroelastosis

Figure 7. Expression of CD90 in human lungs and effects of metformin on TGF β 1-treated human pleural mesothelial cells. A. Serial sections of human pleural/subpleural areas from normal control, idiopathic pulmonary fibrosis (IPF), apical cap (pleural fibrosis near lung bulla), and idiopathic pleuroparenchymal fibroelastosis (PPFE): H&E staining; immunohistochemistry using anti-SMA antibody; immunohistochemistry using anti-CD90 antibody. P, pleura; Sub, subpleural area. Scale bars: 50 μ m (\times 200). B. Quantitative PCR using cDNA samples from cultured human mesothelial cells (Met-5A). Met-5A cells were treated with or without metformin after TGF β 1 administration. Data represent mean values \pm standard deviations of the results obtained from three independent experiments performed in triplicate. Statistical analyses were performed using one-way analyses of variance with Bonferroni correction. * P <0.05, ** P <0.01, *** P <0.01.

Table 3. Comparison of mouse pleural fibrosis model with human pleuroparenchymal fibroelastosis (PPFE)

	Mouse pleural fibrosis model	Human PPFE
Morphologic feature		
Pleural fibrosis	Very severe	Moderate to severe
Pleural elastosis	Severe	Moderate to severe
Subpleural fibrosis	Mild	Severe
Subpleural elastosis (intra-alveolar fibroelastosis)	Few	Very severe
Inflammation	Mild (mainly due to T cells)	Few
Immunoreactivity on fibroblast-like cells in fibrotic pleura		
α SMA	Positive	Positive
CD90	Positive	Positive
WT1	Both positive and negative	Negative*
Podoplanin	Negative	Positive*

*, Based on our previous observation [27].

in mouse fibrotic pleura, the mesothelial cell marker WT1 was positive on pleural myofibroblasts at the external area near the mesothelium and negative on those at the internal area near the pleural elastic layer (**Figure 8**), suggesting the presence of subpopulations in pleural myofibroblasts. It remains necessary to further evaluate the origin of pleural CD90^{pos} (myo)fibroblasts using lineage-tracing mouse lines such as those with a *Wt1-creER* driver for mesothelial cells and a *Pdgfra-creER* driver for fibroblasts.

We found an increase in CD90^{pos} myofibroblasts in human fibrotic pleura (**Figure 7A**). Interestingly, a similar cell population is found in the fibrotic peritoneum of patients undergoing long-term peritoneal dialysis [33]. As metformin has been shown to ameliorate peritoneal fibrosis by suppressing MMT in 'peritoneal' mesothelial cells [34], it is reasonable to hypothesize that this drug may also suppress MMT in 'pleural' mesothelial cells. This hypothesis is supported by our finding that metformin suppresses *SNAI1* expression in TGF β 1-treated human pleural mesothelial cells (**Figure 7B**). Metformin is known to inhibit the TGF β -SMAD pathway by AMPK activation and AMPK-inde-

pendent anti-dimerization of TGF β receptor type 2 [35, 36]. Therefore, this drug has the potential to suppress not only the MMT process but also activation of (myo)fibroblasts after MMT. Indeed, in our *in vitro* studies, metformin treatment significantly reduced ECM-related gene expression in cultured mouse CD90^{pos} (myo)fibroblasts (**Figure 6E**) and post-TGF β 1-treated human mesothelial cells (**Figure 7B**), both of which would have undergone MMT before metformin administration. These mechanisms appear to account for the anti-pleural fibroelastosis effect of metformin in our study.

Fibrosis is one of the chief cellular events in inflammatory processes and wound healing. However, persistent chronic inflammation leads to deleterious fibrosis [37]. Besides its anti-fibrotic effects, metformin may play a role in regulating inflammation. It has been reported to exert anti-inflammatory effects by inhibiting the functions of neutrophils and macrophages and inducing apoptosis in macrophages [38], which in turn inhibits the production of inflammatory cytokines and prevents the differentiation of monocytes into macrophages [39, 40]. Further investigation is necessary to evaluate whether the anti-inflammatory effect of

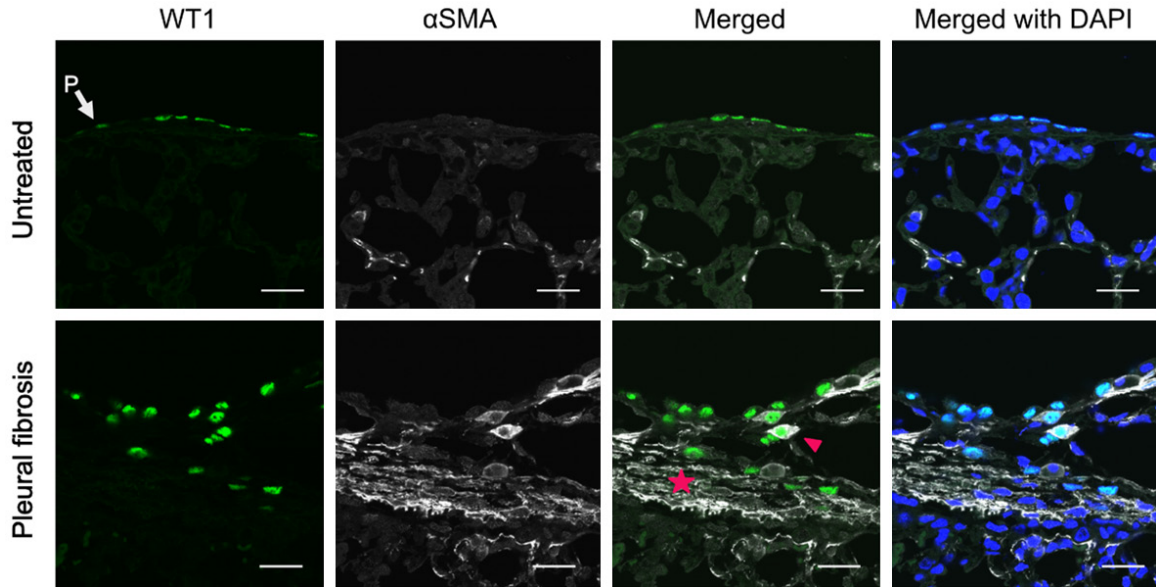


Figure 8. Immunofluorescence on pleural/subpleural area of mouse lungs. High magnification images of a normal lung (upper panels) and a lung from the pleural fibrosis model on day 21 (lower panels) using anti-WT1 antibody (green); anti- α SMA antibody (white) and merged images with or without DAPI (blue). P, pleura. A triangle and a star indicate WT1-positive and WT1-negative myofibroblasts, respectively. Scale bars: 20 μ m (\times 630).

metformin contributes to its anti-pleural fibrosis effect.

In summary, metformin suppresses pleural fibrosis and elastosis, likely by inhibition of ECM production by CD90^{pos} (myo)fibroblasts in the fibrotic lesion. Our findings suggest that this drug may represent a promising therapeutic agent even against human pleural fibrotic diseases, including PPFE.

Acknowledgements

This work was supported by Grants-in-Aid for Scientific Research C (grant number: 16K08-736) and for Early-Career Scientists (grant number: 20K17238) from the Japan Society for the Promotion of Science. The funder provided financial support to the study, but was not involved in the design of the study, the collection, analysis, and interpretation of data, or in the writing of the manuscript. We thank staffs of Department of Regenerative and Infectious Pathology, Hamamatsu University School of Medicine (Mr. Kaneta, Ms. Kawashima, Ms. Hosoda, and Ms. Muranaka) for their technical assistance.

Disclosure of conflict of interest

None.

Address correspondence to: Yasunori Enomoto and Toshihide Iwashita, Department of Regenerative and Infectious Pathology, Hamamatsu University School of Medicine, 1-20-1 Handayama, Higashi-ku, Hamamatsu, Shizuoka 431-3192, Japan. Tel: +81-53-435-2223; Fax: +81-53-435-2224; E-mail: enomotoy@hama-med.ac.jp (YE); Tel: +81-53-435-2223; Fax: +81-53-435-2224; E-mail: toshiiwa@hama-med.ac.jp (TI)

References

- [1] Distler JHW, Györfi AH, Ramanujam M, Whitfield ML, Königshoff M and Lafyatis R. Shared and distinct mechanisms of fibrosis. *Nat Rev Rheumatol* 2019; 15: 705-730.
- [2] Huggins JT and Sahn SA. Causes and management of pleural fibrosis. *Respirology* 2004; 9: 441-447.
- [3] Travis WD, Costabel U, Hansell DM, King TE Jr, Lynch DA, Nicholson AG, Ryerson CJ, Ryu JH, Selman M, Wells AU, Behr J, Bouros D, Brown KK, Colby TV, Collard HR, Cordeiro CR, Cottin V, Crestani B, Drent M, Dudden RF, Egan J, Flaherty K, Hogaboam C, Inoue Y, Johkoh T, Kim DS, Kitaichi M, Loyd J, Martinez FJ, Myers J, Protzko S, Raghu G, Richeldi L, Sverzellati N, Swigris J and Valeyre D; ATS/ERS Committee on Idiopathic Interstitial Pneumonias. An official American Thoracic Society/European Respiratory Society statement: update of the international multidisciplinary classification of

- the idiopathic interstitial pneumonias. *Am J Respir Crit Care Med* 2013; 188: 733-748.
- [4] Reddy TL, Tominaga M, Hansell DM, von der Thusen J, Rassl D, Parfrey H, Guy S, Twentyman O, Rice A, Maher TM, Renzoni EA, Wells AU and Nicholson AG. Pleuroparenchymal fibroelastosis: a spectrum of histopathological and imaging phenotypes. *Eur Respir J* 2012; 40: 377-385.
- [5] Watanabe K, Ishii H, Kiyomi F, Terasaki Y, Hebisawa A, Kawabata Y, Johkoh T, Sakai F, Kondoh Y, Inoue Y, Azuma A, Suda T, Ogura T, Inase N and Homma S; Study Group on Diffuse Pulmonary Disorders, Scientific Research/Research on Intractable Diseases in Japan. Criteria for the diagnosis of idiopathic pleuroparenchymal fibroelastosis: a proposal. *Respir Investig* 2019; 57: 312-320.
- [6] Nakamura Y, Mori K, Enomoto Y, Kono M, Sumikawa H, Johkoh T, Colby TV, Yasui H, Hozumi H, Karayama M, Suzuki Y, Furuhashi K, Fujisawa T, Enomoto N, Inui N, Kaida Y, Yokomura K, Koshimizu N, Toyoshima M, Imokawa S, Yamada T, Shirai T, Nakamura H, Hayakawa H and Suda T. Prognostic and clinical value of cluster analysis in idiopathic pleuroparenchymal fibroelastosis phenotypes. *J Clin Med* 2021; 10: 1498.
- [7] Oda T, Ogura T, Kitamura H, Hagiwara E, Baba T, Enomoto Y, Iwasawa T, Okudela K, Takemura T, Sakai F and Hasegawa Y. Distinct characteristics of pleuroparenchymal fibroelastosis with usual interstitial pneumonia compared with idiopathic pulmonary fibrosis. *Chest* 2014; 146: 1248-1255.
- [8] Enomoto Y, Nakamura Y, Satake Y, Sumikawa H, Johkoh T, Colby TV, Yasui H, Hozumi H, Karayama M, Suzuki Y, Furuhashi K, Fujisawa T, Enomoto N, Inui N, Iwashita T, Kuroishi S, Yokomura K, Koshimizu N, Toyoshima M, Imokawa S, Yamada T, Shirai T, Hayakawa H and Suda T. Clinical diagnosis of idiopathic pleuroparenchymal fibroelastosis: a retrospective multicenter study. *Respir Med* 2017; 133: 1-5.
- [9] Fujisawa T, Mori K, Mikamo M, Ohno T, Kataoka K, Sugimoto C, Kitamura H, Enomoto N, Egashira R, Sumikawa H, Iwasawa T, Matsushita S, Sugiura H, Hashisako M, Tanaka T, Terasaki Y, Kunugi S, Kitani M, Okuda R, Horiike Y, Enomoto Y, Yasui H, Hozumi H, Suzuki Y, Nakamura Y, Fukuoka J, Johkoh T, Kondoh Y, Ogura T, Inoue Y, Hasegawa Y, Inase N, Homma S and Suda T. Nationwide cloud-based integrated database of idiopathic interstitial pneumonias for multidisciplinary discussion. *Eur Respir J* 2019; 53: 1802243.
- [10] Kheirollahi V, Wasnick RM, Biasin V, Vazquez-Armendariz AI, Chu X, Moiseenko A, Weiss A, Wilhelm J, Zhang JS, Kwapiszewska G, Herold S, Schermuly RT, Mari B, Li X, Seeger W, Günther A, Bellusci S and El Agha E. Metformin induces lipogenic differentiation in myofibroblasts to reverse lung fibrosis. *Nat Commun* 2019; 10: 2987.
- [11] Rangarajan S, Bone NB, Zmijewska AA, Jiang S, Park DW, Bernard K, Locy ML, Ravi S, Deshane J, Mannon RB, Abraham E, Darley-Usmar V, Thannickal VJ and Zmijewski JW. Metformin reverses established lung fibrosis in a bleomycin model. *Nat Med* 2018; 24: 1121-1127.
- [12] Li L, Huang W, Li K, Zhang K, Lin C, Han R, Lu C, Wang Y, Chen H, Sun F and He Y. Metformin attenuates gefitinib-induced exacerbation of pulmonary fibrosis by inhibition of TGF- β signaling pathway. *Oncotarget* 2015; 6: 43605-43619.
- [13] Sato N, Takasaka N, Yoshida M, Tsubouchi K, Minagawa S, Araya J, Saito N, Fujita Y, Kurita Y, Kobayashi K, Ito S, Hara H, Kadota T, Yanagisawa H, Hashimoto M, Utsumi H, Wakui H, Kojima J, Numata T, Kaneko Y, Odaka M, Morikawa T, Nakayama K, Kohroggi H and Kuwano K. Metformin attenuates lung fibrosis development via NOX4 suppression. *Respir Res* 2016; 17: 107.
- [14] Xiao H, Huang X, Wang S, Liu Z, Dong R, Song D and Dai H. Metformin ameliorates bleomycin-induced pulmonary fibrosis in mice by suppressing IGF-1. *Am J Transl Res* 2020; 12: 940-949.
- [15] Cavaglieri RC, Day RT, Feliers D and Abboud HE. Metformin prevents renal interstitial fibrosis in mice with unilateral ureteral obstruction. *Mol Cell Endocrinol* 2015; 412: 116-122.
- [16] Xiao H, Ma X, Feng W, Fu Y, Lu Z, Xu M, Shen Q, Zhu Y and Zhang Y. Metformin attenuates cardiac fibrosis by inhibiting the TGFbeta1-Smad3 signalling pathway. *Cardiovasc Res* 2010; 87: 504-513.
- [17] Tripathi DM, Erice E, Lafoz E, García-Calderó H, Sarin SK, Bosch J, Gracia-Sancho J and García-Pagán JC. Metformin reduces hepatic resistance and portal pressure in cirrhotic rats. *Am J Physiol Gastrointest Liver Physiol* 2015; 309: G301-G309.
- [18] Kim JM, Yoo H, Kim JY, Oh SH, Kang JW, Yoo BR, Han SY, Kim CS, Choi WH, Lee EJ, Byeon HJ, Lee WJ, Lee YS and Cho J. Metformin alleviates radiation-induced skin fibrosis via the downregulation of FOXO3. *Cell Physiol Biochem* 2018; 48: 959-970.
- [19] McCloskey CW, Cook DP, Kelly BS, Azzi F, Allen CH, Forsyth A, Upham J, Rayner KJ, Gray DA, Boyd RW, Murugkar S, Lo B, Trudel D, Senterman MK and Vanderhyden BC. Metformin abrogates age-associated ovarian fibrosis. *Clin Cancer Res* 2020; 26: 632-642.
- [20] Decolonne N, Wettstein G, Kolb M, Margetts P, Garrido C, Camus P and Bonniaud P. Bleomy-

- cin induces pleural and subpleural fibrosis in the presence of carbon particles. *Eur Respir J* 2010; 35: 176-185.
- [21] Enomoto Y, Matsushima S, Shibata K, Aoshima Y, Yagi H, Meguro S, Kawasaki H, Kosugi I, Fujisawa T, Enomoto N, Inui N, Nakamura Y, Suda T and Iwashita T. LTBP2 is secreted from lung myofibroblasts and is a potential biomarker for idiopathic pulmonary fibrosis. *Clin Sci (Lond)* 2018; 132: 1565-1580.
- [22] Matsushima S, Aoshima Y, Akamatsu T, Enomoto Y, Meguro S, Kosugi I, Kawasaki H, Fujisawa T, Enomoto N, Nakamura Y, Inui N, Funai K, Suda T and Iwashita T. CD248 and integrin alpha-8 are candidate markers for differentiating lung fibroblast subtypes. *BMC Pulm Med* 2020; 20: 21.
- [23] Akamatsu T, Arai Y, Kosugi I, Kawasaki H, Meguro S, Sakao M, Shibata K, Suda T, Chida K and Iwashita T. Direct isolation of myofibroblasts and fibroblasts from bleomycin-injured lungs reveals their functional similarities and differences. *Fibrogenesis Tissue Repair* 2013; 6: 15.
- [24] Nagendran M, Riordan DP, Harbury PB and Desai TJ. Automated cell-type classification in intact tissues by single-cell molecular profiling. *Elife* 2018; 7: e30510.
- [25] Niethamer TK, Stabler CT, Leach JP, Zepp JA, Morley MP, Babu A, Zhou S and Morrissey EE. Defining the role of pulmonary endothelial cell heterogeneity in the response to acute lung injury. *Elife* 2020; 9: e53072.
- [26] Decologne N, Kolb M, Margetts PJ, Menetrier F, Artur Y, Garrido C, Gauldie J, Camus P and Bonniaud P. TGF-beta1 induces progressive pleural scarring and subpleural fibrosis. *J Immunol* 2007; 179: 6043-6051.
- [27] Enomoto Y, Matsushima S, Meguro S, Kawasaki H, Kosugi I, Fujisawa T, Enomoto N, Inui N, Nakamura Y, Suda T and Iwashita T. Podoplanin-positive myofibroblasts: a pathological hallmark of pleuroparenchymal fibroelastosis. *Histopathology* 2018; 72: 1209-1215.
- [28] Varisco BM, Ambalavanan N, Whitsett JA and Hagood JS. Thy-1 signals through PPAR γ to promote lipofibroblast differentiation in the developing lung. *Am J Respir Cell Mol Biol* 2012; 46: 765-772.
- [29] McGowan SE and McCoy DM. Regulation of fibroblast lipid storage and myofibroblast phenotypes during alveolar septation in mice. *Am J Physiol Lung Cell Mol Physiol* 2014; 307: L618-L631.
- [30] Kretschmer S, Dethlefsen I, Hagner-Benes S, Marsh LM, Garn H and König P. Visualization of intrapulmonary lymph vessels in healthy and inflamed murine lung using CD90/Thy-1 as a marker. *PLoS One* 2013; 8: e55201.
- [31] Kuwahara M, Kuwahara M, Bijwaard KE, Gersten DM, Diglio CA and Kagan E. Mesothelial cells produce a chemoattractant for lung fibroblasts: role of fibronectin. *Am J Respir Cell Mol Biol* 1991; 5: 256-264.
- [32] Wang M, Xiong L, Jiang LJ, Lu YZ, Liu F, Song LJ, Xiang F, He XL, Yu F, Shuai SY, Ma WL and Ye H. miR-4739 mediates pleural fibrosis by targeting bone morphogenetic protein 7. *EBioMedicine* 2019; 41: 670-682.
- [33] Yáñez-Mó M, Lara-Pezzi E, Selgas R, Ramírez-Huesca M, Domínguez-Jiménez C, Jiménez-Heffernan JA, Aguilera A, Sánchez-Tomero JA, Bajo MA, Alvarez V, Castro MA, del Peso G, Cirujeda A, Gamallo C, Sánchez-Madrid F and López-Cabrera M. Peritoneal dialysis and epithelial-to-mesenchymal transition of mesothelial cells. *N Engl J Med* 2003; 348: 403-413.
- [34] Shin HS, Ko J, Kim DA, Ryu ES, Ryu HM, Park SH, Kim YL, Oh ES and Kang DH. Metformin ameliorates the phenotype transition of peritoneal mesothelial cells and peritoneal fibrosis via a modulation of oxidative stress. *Sci Rep* 2017; 7: 5690.
- [35] Yadav H, Devalaraja S, Chung ST and Rane SG. TGF- β 1/Smad3 pathway targets PP2A-AMPK-FoxO1 signaling to regulate hepatic gluconeogenesis. *J Biol Chem* 2017; 292: 3420-3432.
- [36] Xiao H, Zhang J, Xu Z, Feng Y, Zhang M, Liu J, Chen R, Shen J, Wu J, Lu Z, Fang X, Li J and Zhang Y. Metformin is a novel suppressor for transforming growth factor (TGF)-beta1. *Sci Rep* 2016; 6: 28597.
- [37] Wynn TA. Cellular and molecular mechanisms of fibrosis. *J Pathol* 2008; 214: 199-210.
- [38] Cameron AR, Morrison VL, Levin D, Mohan M, Forteath C, Beall C, McNeilly AD, Balfour DJ, Savinko T, Wong AK, Viollet B, Sakamoto K, Fagerholm SC, Foretz M, Lang CC and Rena G. Anti-inflammatory effects of metformin irrespective of diabetes status. *Circ Res* 2016; 119: 652-665.
- [39] Rena G, Hardie DG and Pearson ER. The mechanisms of action of metformin. *Diabetologia* 2017; 60: 1577-1585.
- [40] Juban G, Saclier M, Yacoub-Youssef H, Kernou A, Arnold L, Boisson C, Ben Larbi S, Magnan M, Cuvellier S, Théret M, Petrof BJ, Desguerre I, Gondin J, Mounier R and Chazaud B. AMPK activation regulates LTBP4-dependent TGF- β 1 secretion by pro-inflammatory macrophages and controls fibrosis in duchenne muscular dystrophy. *Cell Rep* 2018; 25: 2163-2176, e6.